Atomic scale interface structure in metallic superlattices

2007 J. Phys.: Condens. Matter 19 136201

(http://iopscience.iop.org/0953-8984/19/13/136201)

IOP PUBLISHING JOURNAL OF PHYSICS: CONDENSED MATTER

J. Phys.: Condens. Matter **19** (2007) 136201 (20pp) doi:10.1088/0953-8984/19/13/136201

Atomic scale interface structure in metallic superlattices

V M Uzdin[1] **and W Keune**[2]

[1] Saint-Petersburg State University, VO 10 Linia 49, 199178, St Petersburg, Russia
[2] Fachbereich Physik, Universität Duisburg-Essen, Lotharstraße 65, D-47048 Duisburg, Germany

Received 10 October 2006, in final form 22 January 2007
Published 12 March 2007
Online at stacks.iop.org/JPhysCM/19/136201

Abstract

We present an atomistic model of interface alloying that presupposes exchange of adatoms with substrate atoms and floating of adatoms on the upper layers during deposition. Due to the existence of a preferred direction (the growth direction), the chemical profile near the interface proves to be asymmetrical. The floating algorithm combined with self-consistent calculations of atomic magnetic moments is used as a model for interpreting Mössbauer data obtained from ^{57}Fe-enriched interfacial tracer layers in Fe/Cr(001) superlattices. The superlattices were grown at different temperatures in order to modify their interface roughness. A linear correlation between calculated moment peaks and observed distinct magnetic hyperfine fields was found. Our experimental samples exhibit larger intermixing than the simplified theoretical model we used. The experimental giant magnetoresistance ratio was observed to increase with the decreasing fraction of certain ^{57}Fe atoms located in the interfacial region. Therefore, bulk scattering from impurity atoms appears to provide the main contribution to the giant magnetoresistance in Fe/Cr. Moreover, our theoretical results clarify the dependence of the short-wavelength period of interlayer coupling on the interface roughness in Fe/Cr.

1. Introduction

The discovery of antiferromagnetic (AF) interlayer exchange coupling (IEC) [1] and giant magnetoresistance (GMR) [2] in Fe/Cr multilayers opened a new field of magnetism, which unites physics, technologies and industrial applications. Despite of the large progress achieved here during the last decade, there are still open questions related to the influence of the atomic scale interface structure on the physical properties [3, 4]. Often the experimental results obtained for the same multilayer structures by different groups as well as the interpretation of these results are in contradiction with each other. Firstly, this is connected with the sensitivity of multilayer properties on the interface roughness and alloying, which sometimes cannot be exactly reproduced even for similar regimes of epitaxial growth. Secondly, most of the

experimental methods give only indirect information about the atomic scale interface structure and, therefore, they need microscopic models for interpretation. The use of different models for the same set of experimental data can lead to contradicting conclusions about the role of the interface roughness in the macroscopic magnetic and transport properties. Taking into account that the study of magnetic multilayers was performed by a number of complimentary experimental methods, the interpretation of all data with a unified microscopic model becomes a problem of great importance. In order to correlate the magnetic properties of multilayers with the conditions of epitaxial growth the theory has to include modelling of the growth process and subsequent self-consistent calculations of the magnetic structure. Then, experimentally measured quantities can be theoretically calculated through the corresponding averaging of atomic scale magnetic moment distributions.

The strong dependence of the magnetic behaviour on the interface structure allows the fabrication of multilayers with the same constitution but with different macroscopic properties. This stimulated the interest to manipulate the interface roughness via *in situ* growth regimes or *ex situ* external action. The typical example here are Fe/Cr structures, which are the most extensively studied metallic multilayer systems. To modify the interface roughness, different research groups used various methods. For sputtered multilayers the interface roughness was governed by the sputtering pressure [5], bilayer number [6], annealing temperature [7–9], and co-deposition of Fe and Cr to increase alloying [8]. In epitaxial samples modification of the interface structure was stimulated by utilizing different substrates [10, 11], special epitaxial regimes with some layers deposited at another temperature [12, 13], ion irradiation [11], introduction of artificially alloyed layers at the interface [10] and annealing [14]. In all cases the variation of interface roughness was accompanied by a change of GMR and (or) IEC. However, the interdependence of macroscopic properties and interface structure proves to be ambiguous, and some of the conclusions declared by different authors were contradictory. Schad *et al* [15] observed a reduction of the GMR effect with increasing amplitude of the interface roughness having constant lateral correlation length. However, later the same group has found that the magnitude of the GMR effect increases with lateral and vertical roughness [14]. They related this contradiction to the polycrystalline structure of the samples [15] and to a large contribution from the bulk scattering to GMR. Fullerton *et al* [16] and later Cyrille *et al* [5, 6] detected an increase of GMR versus interface roughness in sputtered superlattices. Similar observations of magnetoresistance enhancement in annealed and Cr doped multilayers were reported by Rensing *et al* [8]. Kelly *et al* [17] observed an increase of the GMR with increasing roughness induced by ion irradiation. However, Gupta *et al* [11] have found a monotonic decrease of the GMR with increasing of roughness induced by ion irradiation. One of the most elaborate experimental studies of correlation between GMR and interface roughness was performed by Olligs *et al* [18]. They grew high-quality epitaxial Fe/Cr/Fe(001) trilayers and controlled the roughness of the Fe/Cr interface by interrupting the deposition of Fe and Cr at reflection high-energy electron diffraction (RHEED) intensity maxima or minima. The current-in-plane (CIP) GMR of the trilayer with rougher interfaces was found to be significantly enhanced. To connect the GMR with interface or bulk scattering in the multilayers it is necessary to determine the quantitative characteristics of the roughness, which presupposes a microscopic model for rough interfaces. Most of the models consider steps as the main feature of interface roughness. In this case the step height and step density are the vertical and lateral parameters, respectively, of the interface roughness. These characteristics are measured using different experimental methods: x-ray diffraction, analytical transmission electron microscopy, scanning tunnelling microscopy (STM), Mössbauer spectroscopy etc. However, often the reconstruction of the interface structure on an atomic scale remains ambiguous. Most of the approaches determine the step distribution at the interface, but do not take into account interface alloying,

which always exists to some degree and contributes to the effective roughness. Even for the samples grown on an Fe whisker very strong intermixing was detected by scanning tunnelling spectroscopy (STS) for the Cr/Fe(001) (Cr deposited on Fe) interface [19]. It was shown that in the initial stage of deposition only one from every four Cr atoms deposited on the Fe whisker stays at the surface, whereas the other Cr atoms exchange with Fe substrate atoms. Obviously, for the interface with steps the interdiffusion will be even larger, and intermixing will be mostly pronounced near the step edge, where atoms have fewer neighbours [20]. Further, it has been revealed by STS measurements, that intermixing also occurs if Fe is grown on Cr(001) [20]. More recently, a time-dependent STS investigations of Fe growth on Cr(001) showed that the interface is structurally unstable against alloying even at room temperature (RT) [21] Therefore, for an adequate description of the interface structure one has to consider different kinds of roughness, including intermixing, and experimental results obtained by different complimentary methods have to be interpreted on this basis. In their theoretical work Hood *et al* [22] have emphasized the effects of interfacial roughness of Fe/Cr and Fe/Cu multilayers (geometric random roughness, correlated roughness, and varying chemical composition at the interface) on magnetoresistance.

In this paper we treat interface roughness by introducing the scenario of intermixing which presupposes floating of atoms via exchange of adatoms with substrate atoms during the epitaxial growth. In section 2 we describe the stochastic algorithm which realizes such a scenario. In section 3 we present experimental results from Mössbauer spectroscopical and GMR measurements for the Fe/Cr(001) superlattice system containing interfacial ^{57}Fe probe layers, which are used in section 4, together with the intermixing model, for the description of alloying at the interface structure and its correlation with the GMR effect in Fe/Cr superlattices. Finally the paper is concluded in section 5.

2. Model for interface alloying in multilayers

The growth of magnetic multilayers is a complicated process, which depends on a number of factors: deposition rate, growth temperature, roughness and crystallographic orientation of the substrate surface etc. The theoretical description of the surface and interface morphology often uses a self-similarity approach, i.e. the assumption that rescaling of a part of the interface (in general with anisotropy parallel and perpendicular to the growth direction) gives the same interface structure [23]. However, such an approach works only for the description of relatively large systems and failed for magnetic nanostructures. As a rule, their morphology depends on the length scale of observation. Although every spatial scale is characterized by its own type of interface roughness, defects of smaller size often determine the properties of the whole system, even if they cannot be detected at this scale. For example, in metallic Fe/Cr multilayers, as was mentioned above, often steps are considered as the main kind of interface roughness. The characteristic terrace size can be estimated via the average length of the atom's surface diffusion during the evaporation before the next monolayer is deposited. The step width may be up to hundreds of lattice constants or even more. The fraction of the step edge atoms in this case should be quite small. However, as Landes *et al* [24] and Klinkhammer *et al* [25] in their pioneering Mössbauer investigation, and later Schad *et al* [15] and Kopcewicz *et al* [26] have shown, the number of atoms, which are associated with step edge or kink atoms on a stepped interface in traditional models (i.e., dilute Fe–Cr alloy models) for the hyperfine fields [22, 23], is several hundred times larger. It means that on an atomic scale there is another kind of roughness, which cannot be reduced to steps at the interface. STS measurements with atomic resolution show that this kind of roughness is interface alloying [19–21]. Obviously the degree of alloying is connected with the step density, because atoms at the step edge are more flexible

for atomic exchange processes. Moreover, recent calculations show that a size-dependent mesoscopic mismatch, which exists even in homoepitaxy, could give a profound effect on growth modes [27]. Therefore, during the epitaxial growth intermixing can be different when the layer is almost filled and half-filled.

As reported below, for the description of multilayer magnetic properties we model a non-homogeneous interface structure and then perform self-consistent calculations of magnetic moments at each atomic site. Thus we are working at the atomic scale, where exchange of atoms and intermixing are the main forms of interface roughness. We use a supercell with relatively small lateral size ($N = 8 \times 8$ atomic sites) and periodic boundary conditions. Interface defects on a larger scale such as steps, islands and massive embedded clusters are negligible on this scale.

The simplest approach, which describes interface alloying, is the algorithm of ballistic deposition. It produces a very narrow interface, where only two atomic layers in the superlattice contain atoms of both elements [28, 29]. Such a structure of the interface does not agree with experimental results on magnetic moments and hyperfine fields (hff) in most metallic multilayers [30–32]. Moreover, experimentally it was discovered that in superlattices and trilayers A/B growth of element A on substrate B and element B on substrate A is essentially different [10, 32–34]. To model this difference we suggested another stochastic algorithm, which presupposes floating of atoms on the surface of the sample during the epitaxial growth [35–37]. It assumes the exchange of deposited atoms with substrate surface atoms, but forbids internal atomic exchange below the surface. Thus substrate atoms can float up several atomic layers, but newly deposited atoms cannot penetrate deeply into the substrate. Such a scenario of intermixing was proven to exist for thin Cr overlayers on Fe(100) substrates by using proton and electron-induced Auger spectroscopy [38]. It was also confirmed in STS experiments both for Cr deposited on Fe [19] and for Fe deposited on Cr [20, 21]. If the degree of atomic exchange is small, the interface proves to be narrow and almost symmetrical. However, the increase of intermixing leads to the formation of an asymmetrical concentration profile of deposited atoms. The interface becomes abrupt inward of the substrate, but the concentration of substrate atoms decreases exponentially (more slowly for larger exchange parameter) in the direction of growth. Parameters which determine the timescale and consequently the intensity of intermixing are the deposition rate and the temperature of the substrate. Note that epitaxial growth is a non-reversible process, and the probability of atomic exchange usually depends not on the energy of the initial and final state, but on the threshold, which separates these states.

For modelling of intermixing in surface layers during growth we used the following algorithm. We start from the structure of an ideally smooth interface A/B, and then in each pair of successive layers, starting from the bottom, we exchange a defined ratio ζ of randomly chosen atoms. Thus the number of exchanged atoms is the only parameter of the algorithm. It can be taken differently for A on B and B on A interfaces and for different regimes of the sample growth.

In order to determine the concentration profile, produced by such modelling, we will consider the superlattice with nominal structure A_n/B_m and suppose that the probability of atomic exchange ζ is the same for A and B atoms. Denote by $x_A(0)$ the fraction of A atoms in the last B layer at the top of the sample before the deposition of A slab. After deposition of the first A layer we will have on the surface: $x_A(1) = 1 - \zeta(1 - x_A(0))$. Analogously, when all n A layers will be deposited, $x_A(n) = 1 - \zeta^n(1 - x_A(0))$. Then after deposition of m B layers we will have: $x_A(n + m) = 1 - \{1 - \zeta^m[1 - \zeta^n(1 - x_A(0))]\}$. If the boundary effects can be neglected, then $x_A(n + m) = x_A(0)$. This gives the following distribution of A atoms in the superlattice:

$$x_{\mathrm{A}}(k) = 1 - \zeta^k\,(1-\zeta)\,\frac{1-\zeta^m}{1-\zeta^{n+m}} - \zeta\,\delta_{k,n}, \qquad k \leqslant n \tag{1}$$

$$x_{\mathrm{A}}(k) = \zeta^{k-n}\,(1-\zeta)\,\frac{1-\zeta^n}{1-\zeta^{n+m}} + \zeta\,\delta_{k,n+m}, \qquad n < k \leqslant n+m. \tag{2}$$

The equations (1) and (2) give the concentration of A atoms in the nominal A and B layers, respectively. The last terms in both formulae contain the Kronecker symbol $\delta_{k,n}$ ($\delta_{k,n+m}$). They describe the additional appearance (disappearance) in the interface layer of A atoms after switching the deposition from atoms A to B and back. Although the fraction of A atoms in B slabs decreases with distance from the interface, for a fixed layer k_0 it depends non-monotonically on the exchange parameter ζ. For thick A and B slabs the maximum will be at $\zeta = k_0/(k_0+1)$. For larger ζ, most of the atoms which reached layer k_0 continue to flow up and finally will be stopped only at higher layers. The factors $(1-\zeta^n)/(1-\zeta^{n+m}) < 1$ in equation (1) and $(1-\zeta^m)/(1-\zeta^{n+m}) < 1$ in equation (2) take into account the finite thickness of A and B slabs. Some atoms floating into the A slab from lower layers prove to be A atoms, which transfer through the B slab. The number of these atoms increases for thinner B slabs.

If the thickness of slabs B in the superlattice is large, atoms A will flow up inside B layers, but they will not reach the next B slab. The concentration of A atoms in the B layers will decrease monotonically from the maximum value at the B on A interface toward zero and then will jump from 0 to ζN at the A on B interface (where N is the number of atoms in one atomic layer). The total number of A atoms in the B slab will be equal to $2\zeta N$, and half of these atoms are placed at the last B layer, whereas the other atoms form an exponential tail inside the B slab, starting from the first B layer. If $\zeta \ll 1$, interfaces B/A and A/B are almost symmetrical and very narrow. The distribution of A atoms becomes more homogeneous with the intermixing parameter ζ. In the limited case $\zeta \approx 1$ all atoms of the upper substrate layer A will flow up through the B slab as a whole, and interfaces will be again ideally flat. Such floating of Ag atoms through Fe on the surface of the sample was observed in Ag/Fe multilayers using STS [39]. For large ζ, finite thickness of the A and B slabs, taken into account in equations (1) and (2), as well as boundary effects, which were neglected there, are quite important. Note, however, that in all cases the total number of the A atoms in B layers and of B atoms in A layers does not exceed $2\zeta N$. If during the epitaxial growth steps, islands and other large scale defects have been formed on the surface, the number of floated atoms can be larger. Moreover these defects can play the role of the source of dissolved atoms, similar to the formation of bubbles at microscopic defects on the bottom of a pan with boiling water.

The observation of intermixing and alloying at buried interfaces in multilayers can be achieved by different methods, but most of them are indirect, through the measurement of multilayer characteristics, which depend on the interface structure. Only STS gives a real space image of the surface at atomic scale. However, what will happen with this surface after deposition of the subsequent layers can only be estimated from the comparison of the surface structure before and after deposition. Other experimental methods, as a rule, need a model for interpretation and extraction of information about the interface structure. We will focus now on Mössbauer spectroscopy for testing the intermixing algorithms introduced above.

3. Mössbauer spectroscopy on Fe/Cr(100) superlattices

In superlattices with Fe magnetic layers intermixing at the interface may be characterized through a measurement of the relative contributions of different spectral lines in Mössbauer spectra. The distribution $P(B_{\mathrm{hf}})$ of magnetic hff in Fe/Cr structures contains several distinct peaks. The position of these peaks is almost independent of the type of Fe/Cr structure and type

of preparation [31]. If each of these peaks is associated with a specific atomic environment, then Mössbauer spectra can give useful information about the local structure and intermixing at buried interfaces. In previous reports [24–26, 40] satellite lines were interpreted as originating from the non-equivalent Fe sites at the stepped Fe/Cr interface. Different authors used various phenomenological expressions to correlate hff peaks with the numbers of nearest (nn) and next nearest (nnn) Cr neighbours of Fe atoms. Some authors postulated that each nn or nnn Cr atom reduces the magnitude of the hff only [24, 26]. Others presumed for Fe atoms in the atomic layer below the ideally flat Fe/Cr(001) interface that a larger hff than that in bulk Fe exists [25, 40]. In fact, calculations for ideal Fe/Cr(001) interfaces give a magnetic moment of such subsurface Fe atoms which is slightly larger than that of bulk Fe atoms [31, 41].

3.1. Experimental procedures

Fe/Cr(001) superlattices were epitaxially grown by ultrahigh-vacuum deposition of high-purity metals (Fe of natural isotopic composition (^{nat}Fe): 99.9985 at.% purity; ^{57}Fe of 95% isotopic enrichment: 99.95 at.% purity; Cr: 99.999 at.% purity) on epipolished Mg(001) substrates. Details of the preparation were reported earlier [31]. First a 50 Å thick Cr buffer layer was grown on MgO at a substrate temperature, T_S, of ∼900 K. All superlattices studied here had the same composition:

$$\mathrm{MgO/Cr(50\ \text{Å})/[^{57}Fe(3\ ML)/^{nat}Fe(8\ ML)/^{57}Fe(3\ ML)/Cr(8\ ML)]} \times 10.$$

The multilayer period was repeated 10 times. This means that 3 ML (monolayers) thick ^{57}Fe probe layers were artificially placed at both types of interfaces (Fe deposited on Cr (=Fe/Cr, 'lower' interface) and Cr deposited on Fe (=Cr/Fe, 'upper' interface)). The probe layer method [33] is isotope selective and provides an ^{57}Fe nuclear resonance (Mössbauer) signal predominantly from ^{57}Fe atoms in the interface region. In order to change the interface roughness on an atomic scale various superlattices were grown at six different substrate temperatures $T_S(= T_{prep})$, with T_S = 113, 273, 433, 493, 533 and 593 K, respectively. The superlattice structure was characterized by conventional (θ–2θ) low-angle and high-angle x-ray diffraction (XRD). The samples generally exhibited first- and second-order low-angle superstructure Bragg peaks and intensity oscillations from total thickness interference, demonstrating good multilayer quality and flat surfaces [31]. In high-angle XRD the (200) (and no other) Bragg reflection of bcc Fe (and Cr) was detected, proving the single-crystalline (epitaxial) nature of our superlattices [31]. According to the magnetization hysteresis loops (not shown), the samples exhibit zero remanence, i.e. strong antiferromagnetic (AF) interlayer exchange coupling [42]. The CIP (current-in-plane) GMR effect was measured at room temperature (300 K) in external fields B up to 1.1 T by using a conventional four-contact technique. Figure 1 shows the measured dependence of the electrical resistance (top), the change of resistance $\Delta R = [R(B = 0\ \mathrm{T}) - R(B = 1.1\ \mathrm{T})]$ (centre) and the magnetoresistance $\Delta R/R(B = 1.1\ \mathrm{T})$ (bottom) as a function of the growth temperature T_{prep} (or T_S). One can notice that the MR ratio $\Delta R/R$ depend nearly linearly on T_{prep} up to $T_{prep} = 530$ K; above that temperature (at 593 K) the MR ratio is observed to decrease. Conversion electron Mössbauer spectra (CEMS) were measured at room temperature (RT) using a He/CH_4-filled proportional counter and a ^{57}Co source (Rh matrix). The incident γ radiation was perpendicular to the sample surface. The CEM spectra were least-squares fitted by using the NORMOS computer program by Brand [43].

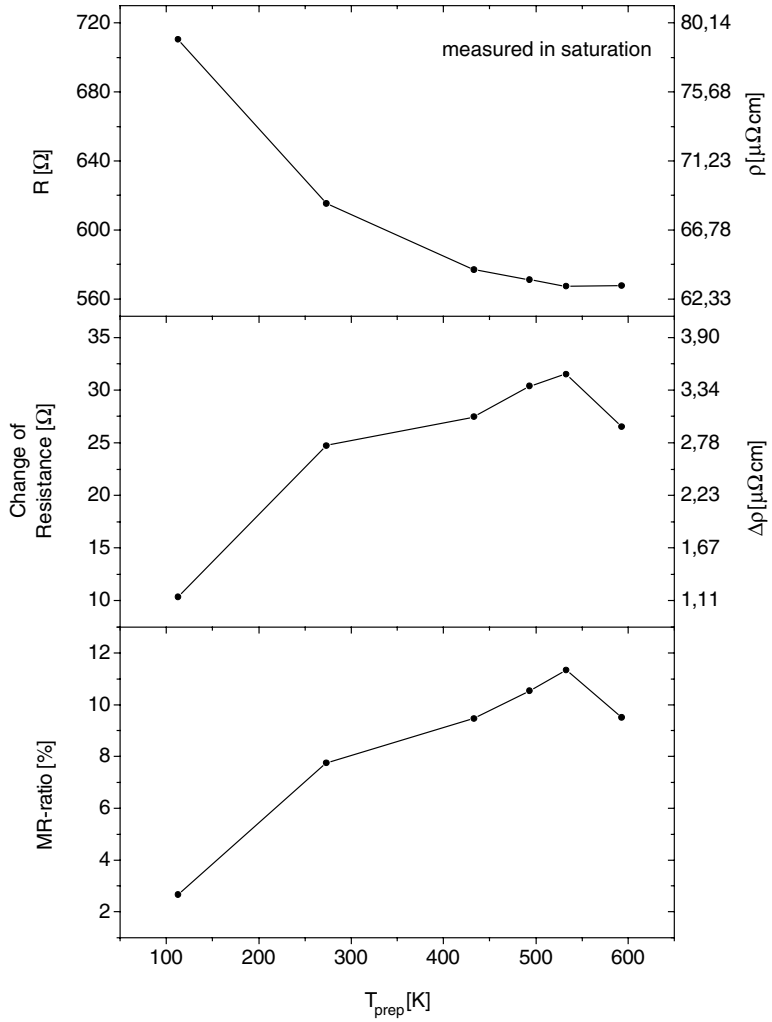

Figure 1. Resistance R (resistivity ρ) (top), change of resistance ΔR (resistivity $\Delta\rho$) (middle) and MR ratio $\Delta R/R$ (bottom) versus the growth temperature T_{prep} of the Fe/Cr(001) superlattice, measured at room temperature. (The lines are a guide for the eye).

3.2. Mössbauer spectroscopy: results and discussion

Typical CEM spectra of two Fe/Cr superlattices, grown at $T_S = 273$ and 593 K, respectively, are shown in figure 2. As compared to the simple Zeeman sextet of ferromagnetic bulk bcc Fe, spectra in figure 2 exhibit distinct shoulders and extra peaks as a result of changes of the ^{57}Fe hff that are induced by neighbouring Cr atoms in the interfacial ^{57}Fe probe layer region. The CEM spectra of the samples grown at other substrate temperatures (not shown) were of similar appearance and statistical quality as the spectra in figure 2.

The measured CEM spectra were least-squares fitted in two different ways. First they were fitted with two hff distributions (not shown), ranging from 0 to 18 T (low-field region) and from 18 to 35 T (high-field region). In order to achieve satisfying fitting, a linear correlation between hff and isomer shift had to be assumed, and, further, the line intensity ratios of the basic

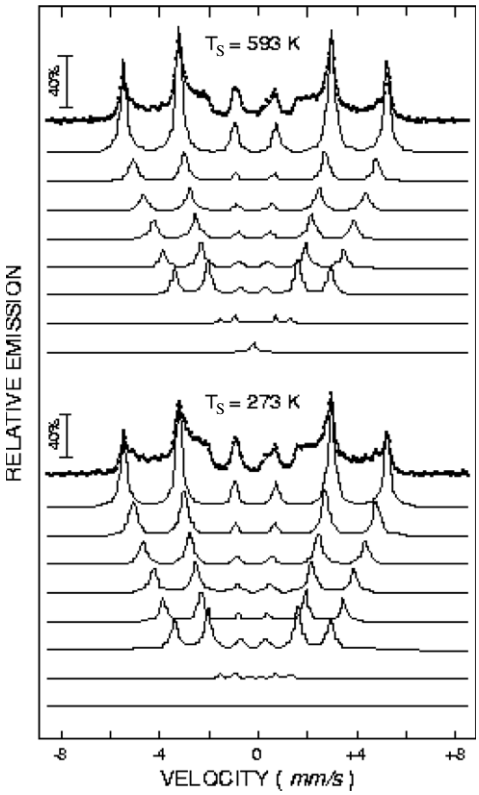

Figure 2. Room temperature CEM spectra of 3 ML thick ^{57}Fe interfacial probe layers in Fe/Cr(001) superlattices grown at $T_S = 593$ K (top) and 273 K (bottom). The line through the data points is the fit curve. Each spectrum was least-squares fitted with a superposition of eight subspectra, as indicated.

sextets in the hff distributions were supposed to be 3:4:1:1:4:3, implying Fe spin orientation in the film plane. As an example, a typical hff distribution, $P(B_{hf})$, of the sample grown at $T_S = 433$ K is shown in figure 5(a) of [31]. $P(B_{hf})$ curves for the other samples grown here are qualitatively similar. The high-field $P(B_{hf})$ distributions of all superlattices exhibit six pronounced maxima, located near $B_{hf} = 33.1$, 30.6, 28.0, 25.2, 22.7, and 19.6 T ($\approx$20 T). Each $P(B_{hf})$ peak originates from a certain characteristic ^{57}Fe environment (site) within or near the Fe–Cr interfacial region [14, 15, 24, 25]. The observed peak positions in the distribution $P(B_{hf})$ were found to be independent of the growth temperature T_{prep} (or T_S). The observed hff value of 33.1 T is equal to the bcc Fe bulk value, at 300 K, and evidently is associated with ^{57}Fe atoms in a 'bulk-like' local environment.

In order to determine the relative occupancies of the different ^{57}Fe sites, a second way of least-squares fitting of the CEM spectra was performed in terms of six different Zeeman-split subspectra (sextets) which correspond to the high-field $P(B_{hf})$ part mentioned above. The Zeeman splittings of these sextets were assumed to be equivalent to the respective hff peak values in the distribution $P(B_{hf})$. Additionally, a sextet with smaller Zeeman splitting plus a central (paramagnetic) single line, corresponding to the low-field $P(B_{hf})$ part, were fitted. All lines had Lorentzian shape, and a line intensity ratio of 3:4:1:1:4:3 was assumed for the sextets, equivalent to in-plane Fe spin orientation. This fitting with discrete subspectra (figure 2) is of

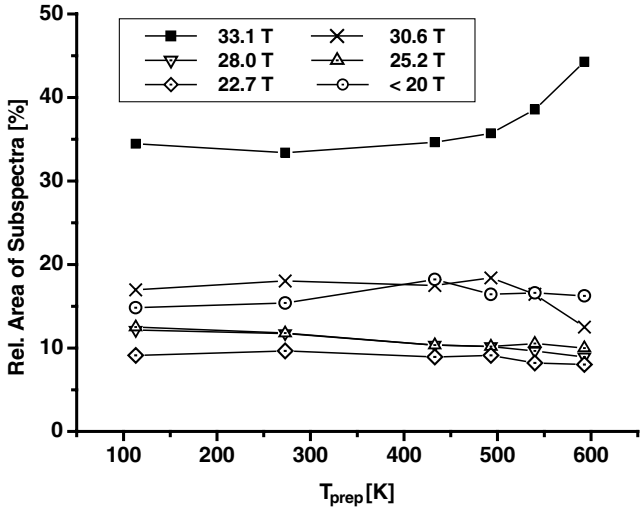

Figure 3. Relative spectral area (relative intensity) of least-squares fitted subspectra (from figure 2) as a function of the growth temperature T_{prep} of Fe/Cr(001) superlattices.

Table 1. Mössbauer subspectrum number, magnetic hyperfine field (hff) B_{hf}, and relative Mössbauer spectral area (relative intensity) for Fe/Cr(001) superlattices grown at $T_{\text{S}} = T_{\text{prep}} = 273$ and 593 K, respectively. Subspectra Nos 1–6 correspond to the high-hff region and subspectra Nos 7, 8 to the low-hff region. (The uncertainty in the relative spectral area is ±0.3%.)

Subspectrum	B_{hf} (T)	$T_{\text{S}} = 273$ K Area (%)	$T_{\text{S}} = 593$ K Area (%)
1	33.1	33.1	43.9
2	30.6	17.9	12.6
3	28.0	11.4	9.0
4	25.2	11.7	9.8
5	22.6	9.6	8.1
6	19.6	14.9	13.7
7	8.8	1.4	2.1
8	0.0	0.01	0.8

similarly good quality as the fitting with a $P(B_{\text{hf}})$ distribution [31]. The relative occupancy of the different ^{57}Fe sites is obtained from the relative spectral area (relative intensity) of each subspectrum (relative to the total spectral area). Results are given in table 1 for our superlattices grown at $T_{\text{S}} = 273$ and 593 K, respectively.

Figure 3 shows the dependence of the relative spectral area of the different subspectra on the growth temperature T_{S} for all samples studied here. The low relative areas of subspectra No 7 and No 8 (low hff region) were added to the relative area of subspectrum No 6 (with $B_{\text{hf}} = 19.6$ T ≈ 20 T), because we associate these three subspectra with Fe atoms which penetrated into the Cr layers to different degrees (see below). Figure 3 demonstrates that there is no drastic change in the contributions of the different subspectra (or in the different Fe site occupancies) below $T_{\text{S}} \approx 450$ K. However, above $T_{\text{S}} \approx 450$ K the bulk contribution (at 33.1 T) increases, whereas the contribution of the next subspectrum (at 30.6 T) is reduced. This is related to stronger intermixing of ^{57}Fe atoms at higher temperatures and with floating of ^{57}Fe atoms from the Fe on Cr interfaces into the Fe slab. The mobility of Cr atoms proves

to be lower [37] than that of Fe atoms, and, consequently, the number of ^{57}Fe atoms which have only a few nn Cr atoms (with $B_{\rm hf} = 30.6$ T) decreases. At $T_{\rm S} = 593$ K, ^{57}Fe atoms with $B_{\rm hf} = 33.1$ and $\leqslant\sim$20 T have the highest occupancies (figure 3). If, according to [15] and [24–26], the relative intensity of the 20 T peak was associated with the number of Fe atoms at the ideally smooth interface, then the area of this peak could be considered as a measure of interface roughness. This, however, would lead to the surprising conclusion that (according to figure 3) interfaces grown at a high substrate temperature are very sharp and have small intermixing. Such a (traditional) interpretation [15, 24–26] is essentially based on the assumption of a linear dependence of the Fe hff on the number of nn and nnn Cr atoms [24, 25]. Our previous work, however, demonstrates that this is not valid for Fe/Cr superlattices, because, although there is strong correlation between measured peak positions in $P(B_{\rm hf})$ and maxima in calculated Fe magnetic moment distributions [29, 31, 44], there is no linear dependence of calculated magnetic moments on the number of Cr neighbours. Moreover, the peak at 20 T was found to correspond to Fe atoms embedded in the Cr layer not far from the interface [31, 44]. Hence, the relatively strong ($\sim$17%) contribution of this line to the total spectrum above 550 K (figure 3) means that there is a considerable number of ^{57}Fe atoms inside the Cr slabs. Therefore, based on our present and earlier [31, 35, 44] results, we adopt a different method of determination of the interface roughness from Mössbauer data as compared to earlier reports by other workers [15, 24–26, 42].

4. Interface structure, exchange coupling and GMR in Fe/Cr multilayers

To relate interface alloying with Mössbauer data we performed a new set of calculations for the distribution of magnetic moments in a ^{57}Fe(3 ML)/^{56}Fe(8 ML)/^{57}Fe(3 ML)/Cr(8 ML) superlattice with intermixing modelled by the 'flow up' algorithm as described in section 2. Monte Carlo simulation of alloying at the interface was repeated 30 times for every pair of intermixing parameters ζ_1 (for Fe on Cr), ζ_2 (for Cr on Fe). Then, for each random structure, self-consistent calculations within the collinear periodic Anderson model (PAM) [28] were performed. Coulomb repulsion of d electrons on site was taken into account in Hartree–Fock approximation. Parameters of the model were chosen to reproduce bulk magnetic properties of ferromagnetic (FM) Fe and AF Cr. It should be mentioned that such an approach was successfully applied for the description of different phenomena in Fe/Cr multilayers with rough interfaces, including the interpretation of Mössbauer [31] and magnetic dichroism spectra [45].

4.1. Interlayer exchange coupling

Our present calculations confirm the existence of the short-wavelength (2 ML) period of IEC oscillations in Fe/Cr multilayers and clarify its dependence on the interface roughness. This is demonstrated in figure 4, where we have plotted the calculated energy difference of antiferromagnetic (AF) and ferromagnetic (FM) states in the superlattice, $\Delta E = E(\text{AF}) - E(\text{FM})$, versus the intermixing parameter ζ_1 for different ζ_2 values. The two-monolayer period of IEC is connected with AF coupling of magnetic moments in successive (100) planes of Fe–Cr and Cr–Cr. As a result, for an odd (even) number of layers in the Cr spacer the IEC has to be FM (AF). Note that in most of the epitaxial and for all sputtered Fe/Cr superlattices the 2 ML period was not observed due to interface roughness. It was detected only in a trilayer grown on an Fe whisker [10], or in samples prepared in special regimes of the epitaxial growth, which ensure very smooth interfaces [12]. But even for these samples the phase of IEC oscillations was found to be opposite to the phase predicted theoretically [12]. Recently this was explained by slightly different intermixing at Fe/Cr and Cr/Fe interfaces [37]. For most experimental samples only

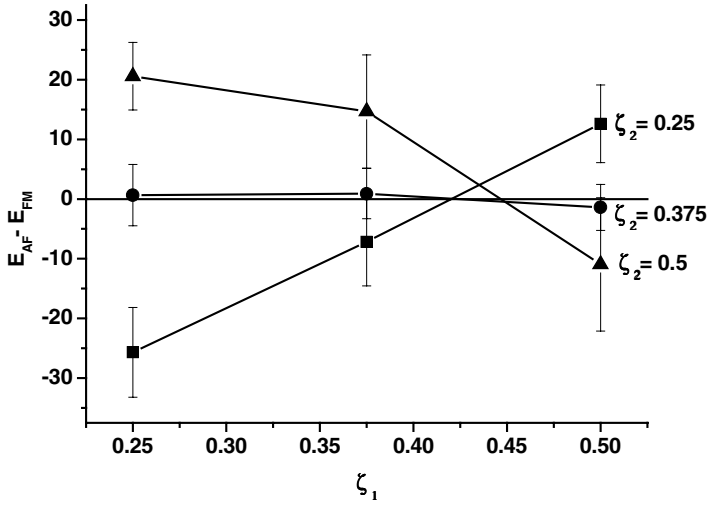

Figure 4. The difference between the energies of AF and FM interlayer coupled states in the Fe/Cr(001) superlattice as a function of atomic intermixing parameters ζ_1 (Fe on Cr) and ζ_2 (Cr on Fe).

the long-wavelength period of IEC can be detected. These oscillations are connected with confinement of free electrons in the quantum wells, formed by magnetic layers. Intermixing in real multilayers with large scale interface roughness (i.e., steps) can be only larger than in the structures without steps and islands which we consider here. Therefore, our model of interface alloying has to describe the behaviour of hff and magnetic moments even in those systems, where the short-wavelength IEC oscillations cannot be observed. At the same time our calculations reproduce the main features of short-wavelength oscillations (figure 4). For equal intermixing parameters (except for the intermediate ζ_2 value) at both interfaces ($\zeta_1 = \zeta_2$) the sign of IEC is found to be the same as for multilayers without alloying. However, if the intermixing at one interface is remarkably larger, the coupling changes its sign (figure 4). The difference in energy, $\Delta E = E_{\mathrm{AF}} - E_{\mathrm{FM}}$, decreases with the intermixing parameter ζ_1 for $\zeta_2 = 0.5$, but increases for $\zeta_2 = 0.25$. It is worth mentioning that for intermediate ζ_2 values ($\zeta_2 = 0.375$) IEC is very small and practically does not depend on the intermixing at the Cr/Fe interface ζ_1. Therefore, depending on the intermixing at the first interface, an increase or decrease of alloying at the other interface can lead to the appearance of AF IEC. Surprisingly, sometimes AF IEC can be caused by additional roughening of one interface (figure 4). Such a behaviour is connected with Cr magnetic moments [37]. The degree of frustration in the intermixed interface region strongly depends on the IEC in the superlattice. As a result the magnetic moments localized on Cr atoms prove to be very different for AF and FM IEC. The state with the higher energy is characterized by a wider distribution of Cr moments and by a larger number of Cr atoms with low moments. This difference disappears when the energies of AF and FM states in the superlattice become close [37].

4.2. Magnetic moment distribution and correlation with B_{hf}

Computed magnetic moments of Fe atoms do not vary drastically with roughness (figure 5). The peak positions in the magnetic moment distribution stay almost unchanged for superlattices with different intermixing ζ_1, ζ_2, and for both types of interlayer coupling. There is, however, a small variation of their relative area. Two typical distributions obtained for $\zeta_1 = \zeta_2 = 0.375$

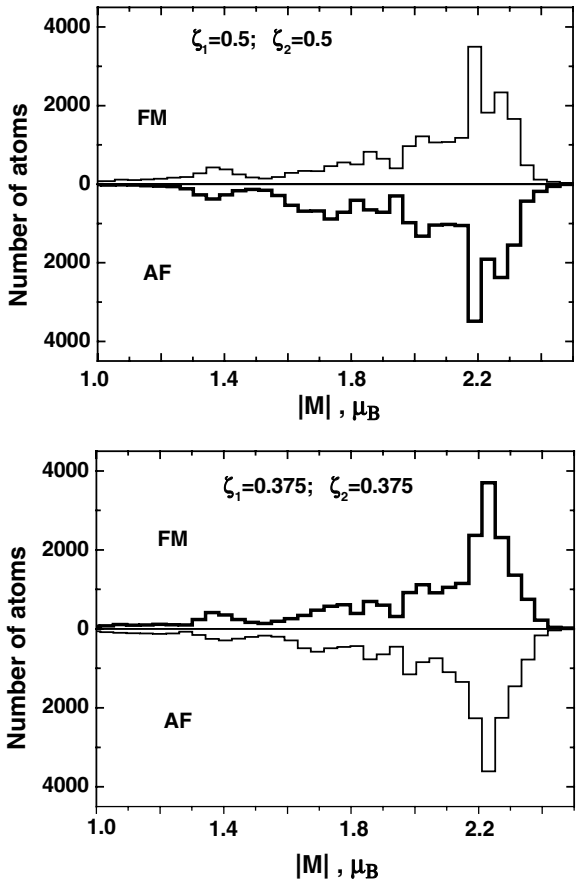

Figure 5. Calculated distributions of magnetic moments on ^{57}Fe atoms in the superlattice ^{57}Fe(3 ML)/^{56}Fe(8 ML)/^{57}Fe(3 ML)/Cr(8 ML) with alloyed interfaces for AF and FM interlayer coupling. Intermixing parameters ζ_1 and ζ_2 are the same for both interfaces. The bold line shows the ground state. Top: $\zeta_1 = \zeta_2 = 0.375$. Bottom: $\zeta_1 = \zeta_2 = 0.5$.

and $\zeta_1 = \zeta_2 = 0.5$ are shown in figure 5. The ground state is marked by a bold line. Since the hyperfine field B_{hf} was found to scale linearly with the calculated magnetic moment [31, 44], the calculated magnetic moment distribution can be used as a model for the interpretation of Mössbauer data. Therefore, it is interesting to compare the distributions of magnetic moments, hyperfine fields and their dependences on the intermixing at the interface. Table 2 demonstrates the evolution of Fe magnetic moments versus ζ_1 and ζ_2 for superlattices with FM and AF interlayer coupling. We show in table 2 the position M of each calculated magnetic moment peak, the corresponding hyperfine field B_{hf} calculated by scaling the magnetic moment M with a factor of 15 T/μ_{B} [46], and the relative areas (%) of the magnetic moment peaks in the calculated moment distribution. (The position of each moment peak was calculated as the mean value between its two neighbouring minima in the moment distribution.) The state with lower energy is emphasized by bold letters. Very good agreement is obtained between the B_{hf} values calculated by scaling (table 2) and the experimentally determined B_{hf} values (table 1). Obviously, the conversion factor of 15.0 T/μ_{B} is applicable in the case of intermixed Fe/Cr interfaces.

Table 2. Results of self-consistent calculations of magnetic moments at ^{57}Fe atoms for superlattices ^{57}Fe(3 ML)/^{56}Fe(8 ML)/^{57}Fe(3 ML)/Cr(8 ML) with interface alloying determined by the parameters ζ_1 and ζ_2. Positions of peaks in magnetic moment distributions (figure 5) M (in μ_B), corresponding B_{hf} values (in T), and relative area (in %) of each peak in the magnetic moment distribution are given for AF and FM interlayer coupling in the superlattice. The state with lower energy is indicated by bold typing.

$\zeta_1 = 0.25$ $\zeta_2 = 0.25$						$\zeta_1 = 0.25$ $\zeta_2 = 0.375$						$\zeta_1 = 0.25$ $\zeta_2 = 0.5$					
AF			FM			AF			**FM**			AF			**FM**		
M	**B_{hf}**	**%**	*M*	B_{hf}	%	*M*	B_{hf}	%	**M**	**B_{hf}**	**%**	*M*	B_{hf}	%	**M**	**B_{hf}**	**%**
2.23	**33.1**	**63.6**	2.24	33.3	61.7	2.23	33.1	61.9	**2.25**	**33.4**	**55.8**	2.24	33.3	55.4	**2.25**	**33.4**	**51.9**
1.98	**29.4**	**5.9**	2.01	29.9	8.4	1.98	29.4	6.9	**2.03**	**30.2**	**13.4**	2.01	29.9	10.1	**2.03**	**30.2**	**13.4**
1.88	**27.9**	**11.6**	1.84	27.4	11.7	1.87	27.8	10.8	**1.89**	**28.1**	**7.6**	1.88	27.9	9.1	**1.88**	**27.9**	**10.4**
1.71	**25.4**	**11.3**	1.68	25.0	5.9	1.68	25.0	11.7	**1.71**	**25.4**	**12.8**	1.67	24.8	16.4	**1.73**	**25.7**	**13.8**
1.18	**17.5**	**7.6**	1.35	20.1	12.3	1.16	17.2	8.7	**1.25**	**18.6**	**10.4**	1.16	17.2	9.0	**1.30**	**19.3**	**10.5**
$\zeta_1 = 0.375$ $\zeta_2 = 0.25$						$\zeta_1 = 0.375$ $\zeta_2 = 0.375$						$\zeta_1 = 0.375$ $\zeta_2 = 0.5$					
AF			FM			AF			**FM**			AF			**FM**		
M	**B_{hf}**	**%**	*M*	B_{hf}	%	*M*	B_{hf}	%	**M**	**B_{hf}**	**%**	*M*	B_{hf}	%	**M**	**B_{hf}**	**%**
2.22	**33.0**	**64.0**	2.23	33.1	60.6	2.23	33.1	58.1	**2.23**	**33.1**	**58.3**	2.24	33.3	50.8	**2.24**	**33.3**	**51.0**
1.98	**29.4**	**6.5**	2.00	29.7	9.8	2.00	29.7	11.3	**2.01**	**29.9**	**11.5**	2.03	30.2	16.0	**2.03**	**30.2**	**15.8**
1.88	**27.9**	**10.5**	1.89	28.0	6.9	1.88	27.9	8.1	**1.88**	**27.9**	**7.1**	1.88	27.9	6.8	**1.88**	**27.9**	**9.5**
1.70	**25.3**	**9.3**	1.67	24.8	16.8	1.69	25.1	12.2	**1.70**	**25.3**	**11.8**	1.68	25.0	18.3	**1.72**	**25.6**	**12.0**
1.39	**20.7**	**4.8**	1.26	18.7	5.9	1.41	21.0	5.5	**1.24**	**18.4**	**11.3**	1.30	19.3	8.1	**1.25**	**18.6**	**11.7**
0.96	**14.3**	**4.9**				1.02	15.2	4.8									
$\zeta_1 = 0.5$ $\zeta_2 = 0.25$						$\zeta_1 = 0.5$ $\zeta_2 = 0.375$						$\zeta_1 = 0.5$ $\zeta_2 = 0.5$					
AF			**FM**			**AF**			FM			**AF**			FM		
M	B_{hf}	%	**M**	**B_{hf}**	**%**	**M**	**B_{hf}**	**%**	*M*	B_{hf}	%	**M**	**B_{hf}**	**%**	*M*	B_{hf}	%
2.22	33.0	64.5	**2.22**	**33.0**	**60.4**	**2.20**	**32.7**	**57.3**	2.22	33.0	57.7	**2.24**	**33.3**	**48.0**	2.24	33.3	48.6
1.98	29.4	7.3	**2.00**	**29.7**	**10.3**	**1.99**	**29.6**	**12.7**	2.00	29.7	12.0	**2.04**	**30.3**	**19.6**	2.04	30.3	19.7
1.87	27.8	9.3	**1.89**	**28.1**	**7.6**	**1.86**	**27.6**	**5.4**	1.88	27.9	7.1	**1.88**	**27.9**	**7.5**	1.88	27.9	8.4
1.68	25.0	7.5	**1.68**	**25.0**	**17.3**	**1.73**	**25.7**	**8.3**	1.67	24.8	16.6	**1.69**	**25.1**	**18.3**	1.70	25.3	10.7
1.24	18.4	11.4	**1.22**	**18.1**	**4.4**	**1.59**	**23.6**	**9.7**	1.22	18.1	6.6	**1.33**	**19.8**	**6.6**	1.24	18.4	12.6
						1.28	**19.0**	**6.6**									

The largest difference between theoretical results in table 2 and experimental data presented in figure 3 is the fraction (%) of the bulk Fe contribution with $M = 2.2\ \mu_B$ and $B_{hf} = 33$ T. The calculations show that generally more than 50% of the Fe atoms have magnetic moments close to the bulk value, although versus intermixing ζ the number of Fe atoms with bulk moments decreases (from 60% to 48%). The relative spectral area of the bulk-like hff in Mössbauer spectra is only about 35% at low T_{prep} values and increases to 45% for the samples grown at 593 K (figure 3). There may be two reasons for this difference. First, our calculations were performed for $T = 0$ K, whereas all measurements were done at room temperature. In general low-temperature measurements show slightly larger B_{hf} values. However, temperature effects are more noticeable for atoms with small magnetic moments and cannot explain the low percentage of the bulk contribution in the experimental spectra. The second reason is the neglect in our calculations of all interface defects (steps, kinks, etc) except atomic scale intermixing. Apparently this leads to an underestimation of the calculated interface roughness as compared to the real samples. For superlattices with ideally flat interfaces, 67% (=2/3) of the ^{57}Fe atoms within 3 ML thick interfaces have no nn Cr atoms. In accordance with *ab initio*

calculations [41] such Fe atoms have magnetic moments close to the bulk value or even larger. Floating of some ^{57}Fe atoms during epitaxial growth decreases the bulk contribution. In fact, ^{57}Fe atoms which float from the Cr on Fe interface will not only appear in the Cr spacer, where their moments will be suppressed, but also expose the underlying ^{57}Fe layers to Cr atoms. This has to decrease the fraction of bulk-like Fe atoms. When ^{57}Fe atoms flow up from the Fe on Cr interface, they pass deeper into the Fe slab. This increases the number of Fe atoms without Cr nn. However, at the same time some Cr atoms, which penetrate into the Fe slab, will compensate this effect. As a result the dependence of the relative spectral area of the bulk-like peak on ζ_2 proves to be larger than its dependence on ζ_1 (see table 2).

Our experimental samples exhibit larger intermixing than the simplified theoretical model we used (compare table 2 with figure 3). The bulk contribution in these samples originates mainly from the Fe on Cr interface [35], and the increase of this fraction at high growth temperature (figure 3) is connected with the diffusion of ^{57}Fe atoms into the Fe slab from this interface. The interdiffusion of Cr atoms may be not so strong, because of the higher cohesive energy of bulk Cr. Magnetic moments of Fe atoms inside the Cr slabs are more sensitive to external conditions, such as proximity of nearest Fe layers, local concentration of FeCr alloy etc. However, despite of the large difference in the local environments of Fe atoms [44, 47], the relative area of different peaks in the calculated magnetic moment distribution changes only slightly (figure 5). A similar behaviour versus growth temperature was observed for the area of the Mössbauer subspectra (figure 3): there is only a small or no change for growth temperatures $\leqslant$450 K.

The interface structure in real superlattices looks more complicated then in our simplified model. Steps and islands at the interface and embedded clusters lead to additional alloying so that intermixing will depend on the lateral position in the superlattice plane. However, on an atomic scale, our model reproduces all the main features of real intermixing, and, further, it makes possible to find the driving force of GMR changes (interface scattering versus bulk scattering) with interface roughness, see below. Despite of the discrepancy in the quantitative relative intensity of different peaks in calculated distributions of magnetic moments M and the measured relative spectral area of different peaks B_{hf}, we can conclude that, in general, the reconstruction of the local interface structure from Mössbauer spectra can be performed. The high-field peaks (at 33.1 and 30.6 T) correspond to ^{57}Fe atoms, which flow up by some monolayers from the Fe on Cr interface into the Fe slabs. Almost all nn of these atoms are Fe atoms. The low-field contributions (at 20 T and below) originate from ^{57}Fe atoms in the Cr slabs. They are surrounded mostly by Cr atoms. Intermediate hff (at 28.0, 25.2 and possibly 22.7 T) originate from atoms with several nn Fe and several nn Cr atoms. These are atoms which form the interface in the real sense (having similar numbers of nn Fe and nn Cr atoms) in the superlattice.

The question which Fe neighbourhoods at Fe/Cr(001) interfaces contribute to the hff peaks at 20, 25 and 27–28 T, as well as 30 T is answered by our computational result shown in figure 6. For the calculation, AFM interlayer coupling with roughness parameters of $\zeta_1 = 0.5$ and $\zeta_2 = 0.75$ were assumed. Figure 6 exhibits the calculated number of Fe atoms versus $\mathrm{nn_{Cr}}$ nearest neighbour Cr atoms and $\mathrm{nnn_{Cr}}$ next nearest neighbour Cr atoms surrounding Fe atoms. Figure 6 demonstrates that the Fe atoms that contribute to these hhf peaks are surrounded by a considerable number of Cr neighbours, In particular, the intermediate hyperfine fields at 25 and 27–28 T (and possibly at 22 T) originate from 'floated' interfacial Fe atoms with more than 3–4 $\mathrm{nn_{Cr}}$ plus $\mathrm{nnn_{Cr}}$ Cr atoms. Scattering of electrons in this region is interface scattering, since all other ^{57}Fe atoms are dissolved inside the Fe and Cr slabs, where electrons are involved in 'bulk' scattering.

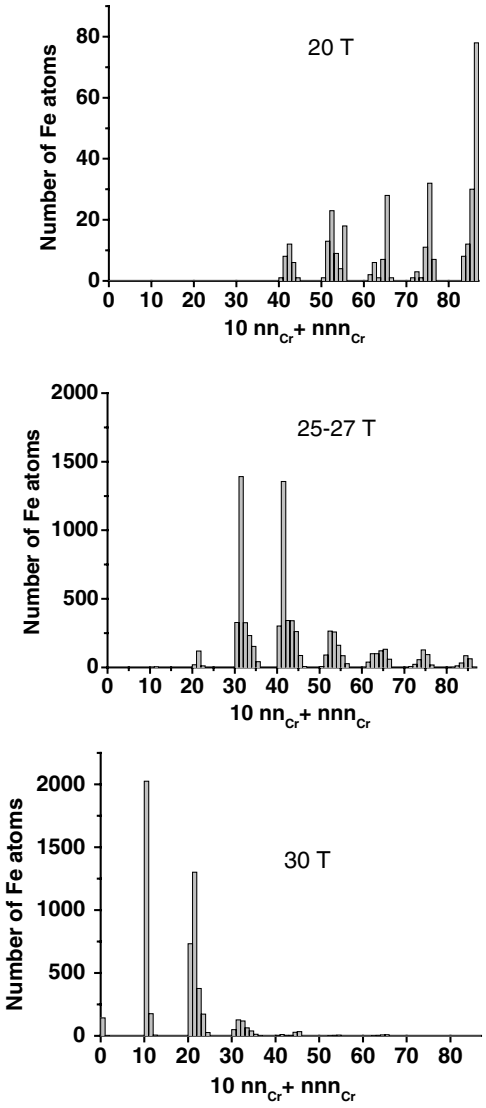

Figure 6. Computed distribution of the number of Fe atoms with nn_{Cr} nearest neighbour Cr atoms and nnn_{Cr} next nearest neighbour Cr atoms, contributing to the hhf peaks at 20 T (top), 25 T + 27 T (middle), and 30 T (bottom). The numbers of the horizontal scale give the value of $10 \times nn_{Cr} + nnn_{Cr}$. For the calculations, interfacial roughness parameters of $\zeta_1 = 0.5$ and $\zeta_2 = 0.75$ were chosen.

4.3. Correlation of magnetoresistance with interface roughness

We can now return to the question about the role of interface scattering and bulk scattering in the formation of GMR. The dependence of the MR ratio on the fraction of 'floated' interfacial ^{57}Fe atoms is shown in figure 7. This fraction of floated interfacial ^{57}Fe was calculated by adding the Mössbauer relative spectral areas of the hff peaks at 25 and 28 T. The number of these floated Fe atoms decreases linearly with the substrate temperature during the epitaxial growth, T_{prep} (figure 3). This leads to a significant increase of the MR ratio (figure 1). Therefore, the bulk

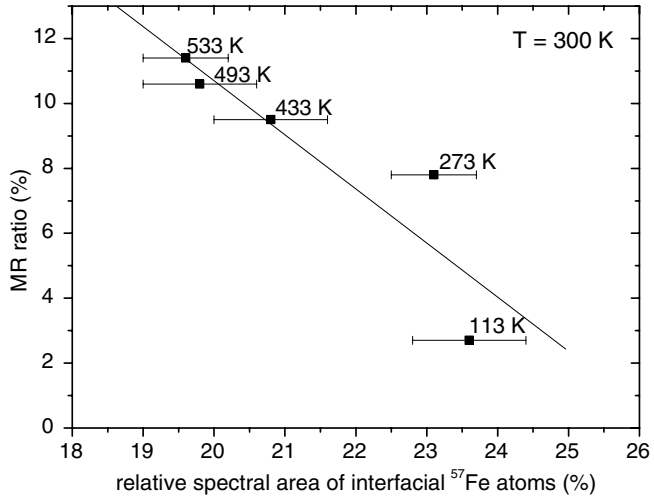

Figure 7. Measured magnetoresistance (MR) ratio versus the relative Mössbauer spectral area (or the fraction) of ^{57}Fe atoms that are located in the Fe/Cr interfacial region and create the hyperfine magnetic fields B_{hf} of 25 and 28 T. The growth temperature is indicated for each data point. (The straight line is a least-squares fit to the data.)

scattering from impurity atoms (Fe in the Cr slabs and Cr in Fe slabs), which are separated from the interface by a few atomic layers, gives the main contribution to the GMR. This explains the increase of GMR in alloyed and Cr doped samples [8]. In some experiments, however, an enhancement of GMR with interface roughness was reported [5, 6, 18, 48]. We have to underline that the number of intermixed atoms depends on the step density and other kinds of large scale interface roughness. Thus, there is an indirect dependence of the GMR effect on the large scale interface roughness, which hides the physical picture of the phenomena and makes the interpretation of experimental data difficult. A schematic representation of the interface in the superlattice with low and high GMR is shown on figure 8. Note that the moment of Fe atoms embedded in the Cr spacer can be reoriented by an external magnetic field more easily than Fe moments inside Fe slabs. Magnetic moments of Cr atoms inside the Fe film, on the contrary, are more stable because of strong AF Fe–Cr coupling.

For larger intermixing, which takes place at higher growth temperature (593 K), the GMR signal was observed to drop again (figure 1, bottom). As was found by our magnetization experiments [42], this is connected with the loss of AF IEC for these samples. The same reason may explain the drop of the MR ratio with ion irradiation [11] and with annealing at high temperature [26].

The scenario of floating of atoms during the sample growth and the model for calculation of magnetic interface profile can be used for the interpretation of experiments with thin overlayers of Cr/Fe [49] and with Fe films embedded in Cr [50, 51]. Kubik *et al* [50, 51] have measured Mössbauer spectra for ^{57}Fe films of different thicknesses (from 1 to 14 ML) sandwiched between Cr(100) layers. A discontinuity of magnetic properties at a thickness of 6 ML Fe was observed [50]. This looked like interface sharpening, but low-energy electron diffraction (LEED) did not reveal any detectable changes. Therefore, the authors [50] interpret this phenomenon in terms of a coupling change between the Fe film and the Cr layers. It is more probable, however, that peculiarities of interface alloying are responsible for the sudden change of the spectra. Our estimations show that a thickness of 6 ML could be the typical

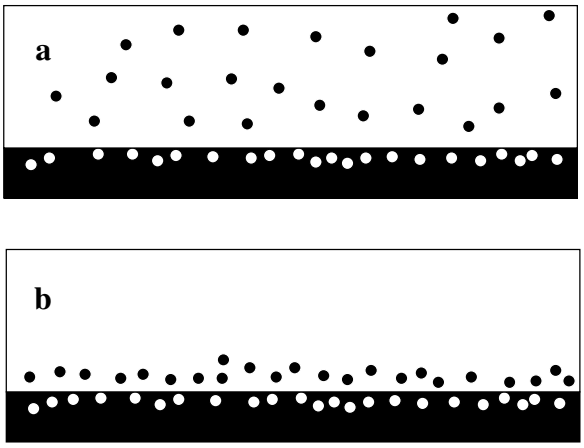

Figure 8. Schematic representation of the interface structure in the multilayers with large (a) and small (b) GMR effect.

Fe slab thickness which Cr atoms cannot overcome during their floating. Thus for thicker Fe slabs the number of Fe atoms without nn Cr atoms increases fast and leads to the formation of the bulk Fe peak in the hff distribution. Note that Fe atoms with only a few nnn Cr (but without nn Cr) have a larger magnetic moment [31, 41], larger hff [25, 40] and therefore, could contribute to the high-field peak. Different hff distributions with larger bulk contributions for Fe on Cr as compared to Cr on Fe interfaces [33] also have a natural explanation within the floating scenario. Further, for thermally annealed Fe/Cr samples our result that the 20 T hff peak is connected with Fe atoms inside Cr layers contradicts the earlier conclusion of other authors [26, 51] that long-range (bulk) diffusion takes place exclusively along (and not perpendicular to) the interfaces, leading to interface smoothing.

4.4. Further discussion of the algorithm of intermixing

It is worthwhile emphasizing that the algorithm of intermixing covers many characteristic features of real film growth, such as, e.g., asymmetry of interfaces, their evolution with a change of the deposition rate, substrate temperature during growth etc, although it contains only one parameter per interface. Most recent theories for the description of interface alloying use parameters which are either estimated from *ab initio* theories or from fitting of experimental data. For the description of intermixing at the Fe/Cr interface Polak *et al* [52] used a model based on composition-dependent, surface enhanced Cr–Fe interactions. Parameters were chosen to fit several data points obtained experimentally and theoretically for bulk alloys. Wille and Dreysse [53] performed Monte Carlo modelling of Fe–Cr alloying for a Cr overlayer on Fe. The relevant interactions were obtained from surface segregation parameters. However, near the surface Cr–Cr and Cr–Fe interactions are quite different from the bulk alloy values. This can be taken into account only very roughly, because accurate *ab initio* calculations exist only for several particular configurations, which presuppose one or two adatoms near the ideal Fe(100) surface [54]. Therefore, the determination of equilibrium energetic parameters is restricted to the low-coverage limit. As for energy barriers separating various lattice sites, which are important for the modelling of epitaxy as a non-equilibrium process, they are almost unknown. Thus all existing theories use a number of parameters and approximations, although their validity often cannot be checked. From this side the theory with only one parameter

for modelling of intermixing proves to be quite attractive. Moreover, this theory can be easily generalized to the case of more elaborate interactions with several phenomenological parameters.

5. Conclusion

Interface alloying is a very general phenomenon, which is always present to some degree during epitaxial growth of metallic multilayers. Atomic scale intermixing is one of the main types of interface roughness, and, therefore, it has to be taken into account for the adequate interpretation of experiments. Here, we presented an atomistic model for the description of interface morphology and interface alloying in terms of the chemical structure on a scale of a few lattice constants. This model presupposes exchange of adatoms with substrate atoms and floating of adatoms on the upper layers during deposition. Due to the existence of a preferred direction—the growth direction—the chemical profile of the interface proves to be different on both sides of the interface. This is the main reason for different alloying on upper and lower interfaces, reported in previous experimental work [10, 32, 33, 55, 56]. We would like to underline that our algorithm describes the intermixing which takes place at the surface of the sample during the deposition. The threshold for exchange of atoms at the surface is essentially lower than for internal diffusion. The degree of alloying depends on the substrate temperature, deposition rate etc, but it always exists in real samples.

Use of the floating algorithm for modelling the interface roughness in Fe/Cr(001) superlattices, combined with self-consistent calculations of atomic magnetic moments, allowed us to calculate magnetic moment distributions for different interface alloying parameters in Fe/Cr. Moreover, the difference between ground state energies of AF and FM interlayer coupled states in the Fe/Cr(001) superlattices as a function of atomic intermixing parameters was calculated. Our results clarify the dependence of the short-wavelength period of interlayer exchange coupling on the interface roughness in Fe/Cr. It is observed that, depending on the intermixing at the first interface, an increase or decrease of alloying at the other interface can lead to the appearance of AF interlayer coupling.

The peak positions in the calculated magnetic moment distributions stay almost unchanged for Fe/Cr superlattices with different intermixing parameters. There is, however, a small variation of the relative peak intensities (relative areas). These calculated results are in qualitative agreement with experimental magnetic hyperfine field distributions at 3 ML thick ^{57}Fe-enriched interfacial probe layers in Fe/Cr(001) superlattices, which were grown at different temperatures, T_{prep}, in order to slightly modify the degree of interdiffusion. A linear correlation of magnetic moment peaks and distinct magnetic hyperfine fields (with a conversion factor of 15.0 T/μ_{B}) was observed. Below $T_{\mathrm{prep}} \approx 450$ K, a small dependence of the relative spectral intensity of hff peaks on T_{prep} was observed. The fraction of floated ^{57}Fe atoms was found to increase with T_{prep}. In principle, the calculated magnetic moment distributions can be used as a model for the interpretation of ^{57}Fe Mössbauer data. Our experimental samples exhibit larger intermixing than the simplified theoretical model we used.

Concerning the role of interface and bulk scattering in GMR, the experimental GMR ratio was observed to increase with the fraction of floated ^{57}Fe atoms, the latter contributing to hff peaks at 33.1, 30.6 and $\leqslant$20 T. Therefore, the bulk scattering from impurity atoms (Fe in Cr slabs and Cr in Fe slabs), which are separated from the interface by a few atomic layers, gives the main contribution to the GMR in Fe/Cr.

The possibility of interpretation of various experimental data on different samples demonstrates that our intermixing model is quite general and can be used as an initial approach for the deduction of chemical and magnetic interface structures. However, steps at the interface,

islands and other large scale defects can essentially change the effective parameters of our algorithm; this can be important for a quantitative comparison with experimental results.

Acknowledgments

The technical assistance of U von Hörsten (Duisburg) is highly appreciated. We thank H Schrör (Duisburg) for performing the measurements. This work was partially supported by DFG-RFBR project 06-02-04005, SFB 491 Bochum/Duisburg, and INTAS-NETWORK project (03-51-4778).

References

[1] Grünberg P, Schreiber R, Pang Y, Brodsky M B and Sowers H 1986 *Phys. Rev. Lett.* **57** 2442
[2] Baibich M N, Broto J M, Fert A, Nguyen Van Dau F, Petroff F, Etienne P, Creuzet G, Friederich A and Chazelas J 1988 *Phys. Rev. Lett.* **61** 2472
[3] Kuch W, Chelaru L I, Offi F, Wang J, Kotsugi M and Kirschner J 2006 *Nat. Mater.* **5** 128
[4] Skubic B, Holmström E, Iusan D, Bengone O, Eriksson O, Brucas R, Hjörvarsson B, Stanciu V and Nordblad P 2006 *Phys. Rev. Lett.* **96** 57205
[5] Cyrille M C, Kim S, Gomez M E, Santamaria J, Leighton C, Krishnan K M and Schuller I K 2000 *Phys. Rev.* B **62** 15079
[6] Cyrille M C, Kim S, Gomez M E, Santamaria J, Krishnan K M and Schuller I K 2000 *Phys. Rev.* B **62** 3361
[7] Hahn W, Loewenhaupt M, Felcher G P, Huang Y Y and Parkin S S P 1994 *J. Appl. Phys.* **75** 3564
[8] Rensing N M, Clemens B M and Williamson D L 1996 *J. Appl. Phys.* **79** 7757
[9] Colino J M, Schuller I K, Korenivski V and Rao K V 1996 *Phys. Rev.* B **54** 1330
[10] Heinrich B, Cochran J F, Monchesky T and Urban R 1999 *Phys. Rev.* B **59** 14520
[11] Gupta A, Paul A, Chaudhari S M and Phase D M 2000 *J. Phys. Soc. Japan* **69** 2182
Gupta A, Paul A, Chaudhari S M and Phase D M 2001 *Vacuum* **60** 401
[12] Schmidt C M, Bürgler D E, Schaller D M, Meisinger F and Güntherodt H-J 1999 *Phys. Rev.* B **60** 4158
[13] Schmidt C M, Bürgler D E, Schaller D M, Meisinger F, Güntherodt H-J and Temst K 2001 *J. Appl. Phys.* **89** 181
[14] Schad R, Belien P, Verbanck G, Moshchalkov V V, Bruynseraede Y, Fischer H E, Lefebvre S and Bessiere M 1999 *Phys. Rev.* B **59** 1242
[15] Schad R, Belien P, Verbanck G, Temst K, Moshchalkov V V, Bruynseraede Y, Bahr B, Falta J, Dekoster J and Langouche G 1998 *Europhys. Lett.* **44** 379
[16] Fullerton E E, Kelly D M, Guimpel J and Schuller I K 1992 *Phys. Rev. Lett.* **68** 859
[17] Kelly D M, Schuller I K, Korenivski V, Rao K V, Larsen K K, Bottiger J, Gyorgy E M and van Dover R B 1994 *Phys. Rev.* B **50** 3481
[18] Olligs D, Bürgler D E, Wang Y G, Kentzinger E, Rücker U, Schreiber R, Brückel Th and Grünberg P 2002 *Europhys. Lett.* **59** 458
[19] Davies A, Stroscio J A, Pierce D T and Celotta R J 1996 *Phys. Rev. Lett.* **76** 4175
[20] Choi Y J, Jeong I C, Park J-Y, Kahng S-J, Lee J and Kuk Y 1999 *Phys. Rev.* B **59** 10918
[21] Ravić R, Bode M and Wiesendanger R 2002 *J. Phys.: Condens. Matter* **15** S2513
[22] Hood R Q, Falicov L M and Penn D R 1994 *Phys. Rev.* B **49** 368
[23] Barabasi A-L and Stanley H E 1995 *Fractal Concepts in Surface Growth* (Cambridge: Cambridge University Press) p 366
[24] Landes J, Sauer Ch, Dörrer S and Zinn W 1992 *J. Magn. Magn. Mater.* **113** 137
[25] Klinkhammer F, Sauer Ch, Tsymbal E Yu, Handschuh S, Leng Q and Zinn W 1996 *J. Magn. Magn. Mater.* **161** 49
[26] Kopcewicz M, Lucinski T, Stobiecki F and Reiss G 1999 *J. Appl. Phys.* **85** 5039
[27] Lysenko O V, Stepanyuk V S, Hergert W and Kirschner J 2002 *Phys. Rev. Lett.* **89** 126102
[28] Kazansky A K and Uzdin V M 1995 *Phys. Rev.* B **52** 9477
[29] Uzdin V M 2000 *Comput. Mater. Sci.* **17** 477
[30] Labergerie D, Westerholt K, Zabel H and Hjörvarsson B 2001 *J. Magn. Magn. Mater.* **225** 373
[31] Uzdin V, Keune W, Schrör H and Walterfang M 2001 *Phys. Rev.* B **63** 104407
[32] Almokhtar M, Mibu K, Nakanishi A, Kobayashi T and Shinjo T 2000 *J. Phys.: Condens. Matter* **12** 9247
[33] Shinjo T and Keune W 1999 *J. Magn. Magn. Mater.* **200** 598
[34] Kalska B, Blomquist P, Häggström L and Wäppling R 2001 *Europhys. Lett.* **53** 395

[35] Uzdin V, Keune W and Walterfang M 2002 *J. Magn. Magn. Mater.* **240** 504
[36] Uzdin V, Labergerie D, Westerholt K, Zabel H and Hjörvarsson B 2002 *J. Magn. Magn. Mater.* **240** 481
[37] Uzdin V M and Demangeat C 2002 *Phys. Rev.* B **66** 092408
[38] Pfandzelter R, Igel T and Winter H 1997 *Surf. Sci.* **377–379** 963
Pfandzelter R, Igel T and Winter H 1997 *Phys. Rev.* B **54** 4496
[39] Bürgler D E, Schmidt C M, Schaller D M, Meisinger F, Hofer R and Güntherodt H-J 1997 *Phys. Rev.* B **56** 4149
[40] Zukrowski J, Liu G, Fritzsche H and Gradmann U 1995 *J. Magn. Magn. Mater.* **145** 57
[41] Coehoorn R 1995 *J. Magn. Magn. Mater.* **151** 341
[42] Schrör H, Keune W, Hosoito N and Shinjo T 1997 *ICMFS '97: Digest of the 15th Int. Colloquium on Magnetic Films and Surfaces (Sunshine Coast, Australia)* unpublished
[43] Brand R A 1987 *Nucl. Instrum. Methods Phys. Res.* B **28** 398
[44] Uzdin V and Keune W 2001 *Phys. Met. Metallogr.* **91** (Suppl. 1) S82
[45] Uzdin V M, Knabben D, Hillebrecht F U and Kisker E 1999 *Phys. Rev.* B **59** 1214
[46] Gubbens P C M, van Apeldoorn J H F, van der Kraan A M and Buschow K H J 1974 *J. Phys. F: Met. Phys.* **4** 921
[47] Uzdin V M 2002 *Comput. Mater. Sci.* **24** 186
[48] Santamaria J, Gomez M E, Cyrille M C, Leighton C, Krishnan K M and Schuller I K 2002 *Phys. Rev.* B **65** 12412
[49] Pfandzelter R, Ostwald M and Winter H 2001 *Phys. Rev.* B **63** 140406
[50] Kubik M, Slezak T, Przybylski M, Karnas W and Korecki J 2001 *Vacuum* **63** 337
[51] Kubik M, Handke B, Karaś W, Spiridis N, Ślęzak T and Korecki J 2002 *Phys. Status Solidi* a **189** 705
[52] Polak M, Fadley C S and Rabinovich L 2002 *Phys. Rev.* B **65** 205404
[53] Wille L T and Dreysse H 1999 *J. Appl. Phys.* **85** 4622
[54] Nonas B, Wildberger K, Zeller R and Dederichs P H 1998 *Phys. Rev. Lett.* **80** 4574
[55] Schurer P J, Celinski Z and Heinrich B 1995 *Phys. Rev.* B **51** 2506
Schurer P J, Celinski Z and Heinrich B 1993 *Phys. Rev.* B **48** 2577
[56] Keavney D J, Wieczorek M D, Storm D F and Walker J C 1993 *J. Magn. Magn. Mater.* **121** 49